Liquid Crystals
Publication details, including instructions for authors and subscription information:
http://www.informaworld.com/smpp/title~content=t713926090

Computer simulation study of a nematogenic lattice model based on an elastic energy mapping of the pair potential

G. R. Luckhurst; S. Romano

Online publication date: 06 August 2010

To cite this Article Luckhurst, G. R. and Romano, S.(1999) 'Computer simulation study of a nematogenic lattice model based on an elastic energy mapping of the pair potential', Liquid Crystals, 26: 6, 871 — 884
To link to this Article: DOI: 10.1080/026782999204561
URL: http://dx.doi.org/10.1080/026782999204561

LIQUID CRYSTALS, 1999, VOL. 26, NO. 6, 871–884

Computer simulation study of a nematogenic lattice model based on an elastic energy mapping of the pair potential

G. R. LUCKHURST*
Department of Chemistry and Southampton Liquid Crystal Institute,
University of Southampton, Southampton SO17 1BJ, UK

and S. ROMANO
Istituto Nazionale per la Fisica della Materia e Dipartimento di Fisica 'A. Volta',
Universitá di Pavia, via A. Bassi 6, I-27100 Pavia, Italy

(*Received 1 December 1998; accepted 11 January 1999*)

Director configurations in a nematic liquid crystal can be determined by minimizing its total elastic free energy, for given elastic constants and specific boundary conditions. In some cases, these configurations have been obtained by numerical procedures where the elastic free energy density plays the same role as the overall potential energy in a standard Metropolis Monte Carlo simulation. The interaction energies or potentials used in these studies are short ranged but, in general, not pairwise additive, unless the three elastic constants are set to a common value, thus reducing the potential to that in the well-known Lebwohl–Lasher lattice model. On the other hand, we can construct, in different ways, a lattice model with pairwise additive interactions, which approximately reproduces the elastic free energy density, where the parameters defining the pair potential are expressed as linear combinations of elastic constants. An anisotropic nematogenic pair interaction of this kind, originally proposed by Gruhn and Hess (T. Gruhn and S. Hess, Z. Naturforsch. A51, 1 (1996)), has recently been investigated by one of us, using a Monte Carlo simulation (S. Romano, Int. J. Mod. Phys. B **12**, 2305 (1998)). Here we propose another approximate procedure for the mapping, and study the resulting pair potential model with the aid of Monte Carlo simulations. The behaviour of the nematic phases formed by the two models is compared together with the predictions of molecular field theory and the properties of the Lebwohl–Lasher model.

1. Introduction

Important aspects of liquid crystal science and technology are related to their elastic properties: for example, they are involved in a number of phenomena where the director is manipulated by external fields, as in display devices, and a knowledge of the elastic behaviour is also important in the study of defects [1]. Thus it is possible to determine director configurations by minimizing the total elastic free energy, for given elastic constants and specific boundary conditions. In a few cases this can be done analytically [2–4], although, in general, numerical methods have been implemented, both static and time-dependent [5–13], usually involving appropriate discretization schemes. That is, the director field is calculated on a discrete grid, usually a lattice of space points, and the partial derivatives defining the elastic free energy density are approximated by finite increments. In this approach, special care is needed in order to ensure that the algorithm preserves the underlying nematic symmetry with respect to inversion of the director field (see, e.g. [9]). Metropolis Monte Carlo approaches have also been used in this context: sometimes the energy minimization was carried out at zero temperature [5, 6], while in other cases a suitably low temperature (well inside the ordered phase) was used, as a means to ensure that the system did not become trapped in a local minimum [7, 8, 12]. The same approach has also been used to investigate the ordering kinetics after quenching from a disordered phase [13]. In all of these calculations, the total elastic free energy density plays the same role as the overall potential energy in a standard Monte Carlo simulation. The potentials used in these investigations are short ranged but, in general, not pairwise

*Author for correspondence. e-mail: gl@soton.ac.uk

Journal of Liquid Crystals ISSN 0267-8292 print/ISSN 1366-5855 online
http://www.tandf.co.uk/JNLS/lct.htm
http://www.taylorandfrancis.com/JNLS/lct.htm

additive, and this makes the simulation rather time consuming; the exception occurs when the three elastic constants are set to a common value, thus reducing the potential to the well-known Lebwohl–Lasher model [14, 15]. This approach has been widely followed in simulation (e.g. Windle and co-workers [5, 6]), and is also rather common in continuum theory [2].

It has also been noted that a pairwise additive interaction can be constructed in different ways, which approximately reproduces the elastic free energy density [6, 12], so that the parameters defining the pair potential are expressed in terms of the elastic constants. For example, a potential model of this kind, originally proposed by Gruhn and Hess [12], has recently been investigated by Monte Carlo simulation [16], under periodic boundary conditions, the aim being to study the microscopic behaviour in bulk. As we shall see, the potential parameters are linear combinations of elastic constants, and so, strictly, the pair potential used depends on temperature because the elastic constants do. Clearly this complicates the identification of the model with a true intermolecular pair potential which is temperature independent. We now want to investigate another possible mapping between the elastic free energy density and the pair potential parameters, and to compare the two approaches starting from a common set of experimental values for the elastic constants. The resulting pair potential is an extension of the Lebwohl–Lasher lattice model, now fully allowing for different values of the elastic constants, and will be used here to investigate the microscopic behaviour of the bulk system. The properties of this will be compared with those of other models and with the predictions of molecular field theory. In the long term, we also intend to use the resulting pair potential to study the elastic and defect behaviour of nematogens.

2. Pair potential models

We recall here the usual expression for the elastic free energy density of achiral nematics [2, 3]

$$g = (1/2)[K_1(\nabla \ \mathbf{n})^2 + K_2(\mathbf{n} \ (\nabla \wedge \mathbf{n}))^2 + K_3(\mathbf{n} \wedge (\nabla \wedge \mathbf{n}))^2], \quad (1)$$

where K_i are the three elastic constants and $\mathbf{n}$ denotes the director. It is also helpful, as we shall see, to have explicit expressions for the terms in g; they are

$$\nabla \ \mathbf{n} = \sum_\alpha \frac{\partial n_\alpha}{\partial x_\alpha}, \quad (\nabla \wedge \mathbf{n})_\alpha = \sum_{\beta,\gamma} \varepsilon_{\alpha\beta\gamma} \frac{\partial n_\gamma}{\partial x_\beta}, \quad (2)$$

where

$$(\nabla \wedge \mathbf{n})_1 = \frac{\partial n_3}{\partial x_2} - \frac{\partial n_2}{\partial x_3}, \quad (\nabla \wedge \mathbf{n})_2 = \frac{\partial n_1}{\partial x_3} - \frac{\partial n_3}{\partial x_1},$$

$$(\nabla \wedge \mathbf{n})_3 = \frac{\partial n_2}{\partial x_1} - \frac{\partial n_1}{\partial x_2} \quad (3)$$

$$\mathbf{n} \ (\nabla \wedge \mathbf{n}) = \sum_\alpha n_\alpha \sum_{\beta,\gamma} \varepsilon_{\alpha\beta\gamma} \frac{\partial n_\gamma}{\partial x_\beta} \quad (4)$$

$$(\mathbf{n} \wedge (\nabla \wedge \mathbf{n}))_1 = n_2(\nabla \wedge \mathbf{n})_3 - n_3(\nabla \wedge \mathbf{n})_2 \quad (5)$$

$$(\mathbf{n} \wedge (\nabla \wedge \mathbf{n}))_2 = n_3(\nabla \wedge \mathbf{n})_1 - n_1(\nabla \wedge \mathbf{n})_3 \quad (6)$$

$$(\mathbf{n} \wedge (\nabla \wedge \mathbf{n}))_3 = n_1(\nabla \wedge \mathbf{n})_2 - n_2(\nabla \wedge \mathbf{n})_1. \quad (7)$$

The coordinate system set in the laboratory is defined by three orthonormal unit vectors $\mathbf{e}_\alpha$, $\alpha = 1, 2, 3$, and the coordinates x_α have the dimension of length. It is convenient, therefore, to transform to dimensionless coordinates, so that the elastic free energy density is now given by $g = \Psi\Lambda^{-2}$, where Λ is an arbitrary length, and the elastic energy stored in the corresponding unit cube is then of order $\Psi\Lambda$ (we note that Ψ is now defined by equations (1) to (7), but with dimensionless coordinates x_α).

As for the pair potential model, we consider here three-component unit vectors $\mathbf{u}_k$ associated with a three-dimensional (simple cubic) lattice, with $\mathbf{p}_k$ denoting the dimensionless lattice-point coordinates. A general even anisotropic interaction potential acting between nearest neighbours can be written as a polynomial, or a power series, in terms of the appropriate combinations of scalar invariants; this gives

$$\Phi = \Phi_{jk} = \text{const} + \tau_2 + \tau_3 + \tau_4 + \ldots \quad (8)$$

with

$$\tau_2 = c_{2,1}(a_j^2 + a_k^2) + c_{2,3} b_{jk}^2, \quad (9)$$

$$\tau_3 = c_{3,1} a_j a_k b_{jk}, \quad (10)$$

$$\tau_4 = c_{4,1}(a_j^4 + a_k^4) + c_{4,2}(a_j a_k)^2 + c_{4,3}(a_j^2 + a_k^2) b_{jk}^2 + c_{4,4} b_{jk}^4. \quad (11)$$

The scalar invariants involving neighbouring unit vectors and the vector joining them are

$$\mathbf{r} = \mathbf{p}_j - \mathbf{p}_k, \quad \mathbf{s} = \mathbf{r}/|\mathbf{r}|, \quad a_j = \mathbf{u}_j \ \mathbf{s}, \quad a_k = \mathbf{u}_k \ \mathbf{s},$$

$$b_{jk} = \mathbf{u}_j \ \mathbf{u}_k; \quad (12)$$

the $c_{h,l}$ denote arbitrary expansion coefficients, and each term τ_h is a homogeneous polynomial of order h. The functional form resulting from the argument developed in [12] (§4.2, especially equations (15) and (16)), corresponds to neglecting all higher order terms τ_h with $h \geqslant 5$, and to setting $c_{4,1} = c_{4,2} = c_{4,4} = 0$, $c_{4,3} \neq 0$. After changing to a more convenient notation for the coefficients, the

pair potential suggested in [12] takes the form

$$\Phi = \Phi_{jk} = \lambda[P_2(a_j) + P_2(a_k)] + \mu\left(a_j a_k b_{jk} - \frac{1}{9}\right) + \nu P_2(b_{jk}) + \rho[P_2(a_j) + P_2(a_k)]P_2(b_{jk}), \quad (13)$$

where $P_2(a_j)$ denotes the second Legendre polynomial. Equation (13) can also be expressed as a linear combination of S-functions [17–19]; for those not familiar with the S-function representation of the pair potential, we give in the Appendix a brief description of the relevant formalism.

The four strength parameters λ, μ, ν, ρ are defined by the following combinations of elastic constants [12], including the factor Λ, so that the strength parameters have the dimension of energy.

$$\begin{cases} \lambda = \frac{1}{3}\Lambda(2K_1 - 3K_2 + K_3) \\ \mu = +3\Lambda(K_2 - K_1) \\ \nu = \frac{1}{3}\Lambda(K_1 - 3K_2 - K_3) \\ \rho = \frac{1}{3}\Lambda(K_1 - K_3). \end{cases} \quad (14)$$

The present expression for the pair potential differs from its counterpart in [12] by multiplicative and additive numerical factors, adjusted so as to make the isotropic average of the potential equal to zero, and to facilitate contact and comparison with the Lebwohl–Lasher model, which corresponds to equal values of the elastic constants, that is $\lambda = \mu = \rho = 0$.

It is helpful to summarize briefly the argument developed in §4.2 of [12]: the authors start from a suitably discretized version of the elastic free energy density, and consider a director field depending on two coordinates only; then their discretized elastic free energy density becomes pairwise additive. After interpreting the resulting equation in terms of scalar products, they propose a pair potential generalizing it; they finally express the potential parameters in terms of elastic constants by considering the energies of just five specific configurations.

A similar model has already been studied in the literature in connection with the simulation of nematic liquid crystals [20], i.e.

$$D_{jk} = \frac{\varepsilon}{r^6}\{(\gamma^2 - \gamma)[P_2(a_j) + P_2(a_k)] + \gamma^2[(9a_j a_k b_{jk} - 1) - P_2(b_{jk}) - 6P_2(a_j)P_2(a_k)]\}. \quad (15)$$

This is the dispersion interaction (or, more precisely, an approximate expression for the dipolar contribution to the dispersion interaction) between two identical axially symmetric molecules, as proposed by London and de Boer [18, 21, 22]; here γ denotes the anisotropy of the polarizability tensor. A lattice model where the interaction is restricted to nearest neighbours produces a nematic-like ordering transition [20]. In contrast, inclusion of next-nearest neighbours produces a ground state structure with sub-lattice order, but no net orientational order [23]. Notice also that most coefficients in equation (15) are proportional to γ^2, so that γ^2 can be absorbed into ε which gives an expression with a weak residual γ dependence. Simulations were carried out with $\gamma = 0.5$, 0.65, 0.80, and, as expected, they yielded very similar results, which were also in agreement with the truncated potential model obtained by neglecting the term proportional to γ. The scaled transition temperature T^*_{NI} for this model is about 2.25, where $T^* = k_B T/(\varepsilon\gamma^2)$, in comparison with a molecular field estimate of 2.6424 [20]. In equation (15), γ is smaller than 1 in magnitude; however, short range potential models defined by $\gamma = 1$ (i.e. polarizability only along the molecular symmetry axis) have been considered in the literature [24, 25].

It is of interest to retain the functional form of the pair potential in equation (8) (of which both equations (13) and (15) are special cases), but to relate the expansion coefficients to the elastic constants rather than the molecular polarizability. To obtain this relationship, we note that, in equation (1), we can, without any loss of generality, define the laboratory frame so that $\mathbf{n} = \mathbf{e}_3 = (0, 0, 1)$ at an arbitrary point, thus

$$\mathbf{n}\ (\nabla \wedge \mathbf{n}) = \frac{\partial n_2}{\partial x_1} - \frac{\partial n_1}{\partial x_2} \quad (16)$$

and

$$(\mathbf{n} \wedge (\nabla \wedge \mathbf{n}))^2 = (\nabla \wedge \mathbf{n})_1^2 + (\nabla \wedge \mathbf{n})_2^2, = \left(\frac{\partial n_3}{\partial x_2} - \frac{\partial n_x}{\partial x_3}\right)^2 + \left(\frac{\partial n_1}{\partial x_3} - \frac{\partial n_3}{\partial x_1}\right)^2. \quad (17)$$

We now consider two neighbouring points $\mathbf{x}'$ and $\mathbf{x}''$, such that $\mathbf{x}'' - \mathbf{x}' = \mathbf{m}$, where $\mathbf{m}$ is a unit vector lying along a cartesian axis (i.e. coinciding with one of the three $\mathbf{e}_\alpha$s), while $\mathbf{n}'$ and $\mathbf{n}''$ denote the corresponding directors, with $\mathbf{n}' = \mathbf{e}_3$ and $\mathbf{n}'' = (\xi, \eta, \zeta)$. We further assume that $\xi \approx 0$, $\eta \approx 0$, $\zeta \approx 1$, thus $|\xi| \gg |1 - \zeta|$, $|\eta| \gg |1 - \zeta|$, in keeping with the requirement that the director orientation changes slowly in a nematic. The derivatives appearing in equations (16) and (17) are then approximated by

$$\frac{\partial n_\gamma}{\partial x_\beta} = \begin{cases} (n''_\gamma - n'_\gamma), & \text{if } \mathbf{m} = \mathbf{e}_\beta \\ 0, & \text{else.} \end{cases} \quad (18)$$

Equations (16) and (17) become therefore, to lowest order:

for $\mathbf{m} = \mathbf{e}_1$,

$$\nabla \quad \mathbf{n} = \xi, \tag{19}$$

$$\mathbf{n} \quad (\nabla \wedge \mathbf{n}) = \eta, \tag{20}$$

$$\frac{\partial n_3}{\partial x_1} = \zeta - 1, \tag{21}$$

$$2\Psi = K_1 \xi^2 + K_2 \eta^2; \tag{22}$$

for $\mathbf{m} = \mathbf{e}_2$,

$$\nabla \quad \mathbf{n} = \eta, \tag{23}$$

$$\mathbf{n} \quad (\nabla \wedge \mathbf{n}) = \xi, \tag{24}$$

$$\frac{\partial n_3}{\partial x_2} = \zeta - 1, \tag{25}$$

$$2\Psi = K_1 \eta^2 + K_2 \xi^2; \tag{26}$$

for $\mathbf{m} = \mathbf{e}_3$,

$$\nabla \quad \mathbf{n} = \zeta - 1, \tag{27}$$

$$\mathbf{n} \quad (\nabla \wedge \mathbf{n}) = 0, \tag{28}$$

$$(\mathbf{n} \wedge (\nabla \wedge \mathbf{n}))^2 = \xi^2 + \eta^2, \tag{29}$$

$$2\Psi = K_3(\xi^2 + \eta^2). \tag{30}$$

We now obtain an analogous set of expressions for the pair potential given in equation (13), by further assuming that one of the two unit vectors is aligned along a lattice axis, say $\mathbf{u}_j = \mathbf{e}_3$, $\mathbf{u}_k = (\xi, \eta, \zeta)$, thus $b_{jk} = \zeta$. Then the expressions for the pair potential simplify (exactly) as follows for the three orientations of the intermolecular vector allowed by the simple cubic lattice:

for $\mathbf{s} = \mathbf{e}_1$,

$$a_j = 0, \quad a_k = \xi,$$

$$\Phi - \Phi_0 = +\frac{3}{2}[(\lambda - \nu + 2\rho)\xi^2 + (-\nu + \rho)\eta^2] - \rho A; \tag{31}$$

for $\mathbf{s} = \mathbf{e}_2$,

$$a_j = 0, \quad a_k = \eta,$$

$$\Phi - \Phi_0 = +\frac{3}{2}[(-\nu + \rho)\xi^2 + (\lambda - \nu + 2\rho)\eta^2] - \rho B; \tag{32}$$

for $\mathbf{s} = \mathbf{e}_3$,

$$a_j = 1, \quad a_k = \zeta,$$

$$\Phi - \Phi_0 = -\left[\frac{3}{2}(\lambda + \nu) + \mu + \frac{9}{2}\rho\right](\xi^2 + \eta^2) + \rho C. \tag{33}$$

Here the quartic polynomials A, B, and C are defined by

$$A = \frac{9}{4}\xi^2(\xi^2 + \eta^2), \quad B = \frac{9}{4}\eta^2(\xi^2 + \eta^2), \quad C = \frac{9}{4}(\xi^2 + \eta^2)^2 \tag{34}$$

and the value Φ_0 corresponds to $\xi = \eta = 0$, i.e. to the two molecules being parallel.

In the limit of small angular displacements, we can identify pairs of corresponding expressions for Ψ and $\Phi - \Phi_0$, respectively; by equating lowest order terms, we obtain

$$\begin{cases} \Lambda K_1 = +\frac{3}{2}(\lambda - \nu + 2\rho) \\ \Lambda K_2 = +\frac{3}{2}(-\nu + \rho) \\ \Lambda K_3 = -\left[\frac{3}{2}(\lambda + \nu) + \mu + \frac{9}{2}\rho\right] \end{cases} \tag{35}$$

We note here that, had higher rank terms been included in the pair potential, then these would also have contributed to the lowest order terms in the expansion, thus introducing more parameters. These expressions connect the three elastic constants and the four parameters in the pair potential; some other assumption must now be made, in order to solve equations (35) with respect to the potential parameters. We choose here to set ρ equal to zero, thus dropping all fourth and higher order terms in equation (8), which gives

$$\begin{cases} \Lambda K_1 = +\frac{3}{2}(\lambda - \nu) \\ \Lambda K_2 = -\frac{3}{2}\nu \\ \Lambda K_3 = -\left[\frac{3}{2}(\lambda + \nu) + \mu\right], \end{cases}$$

i.e.

$$\begin{cases} \lambda = +\frac{2}{3}\Lambda(K_1 - K_2) \\ \nu = -\frac{2}{3}\Lambda K_2 \\ \mu = \Lambda(-K_1 + 2K_2 - K_3); \end{cases} \tag{36}$$

in the S-function language, this choice means dropping S_{422} and S_{242} [17–19] (see the Appendix). The assumption used here, i.e. setting ρ to zero, is not the only one possible (for example, we could think of setting $\lambda = 0$ instead of ρ in equations (35)), but, in the present context, our choice seems to be the most straightforward, since it removes the highest rank term from the expansion of the potential. To conclude, we are now studying a pair potential of the form

$$\Phi = \lambda[P_2(a_j) + P_2(a_k)] + \mu\left(a_j a_k b_{jk} - \frac{1}{9}\right) + \nu P_2(b_{jk}). \tag{37}$$

Note also that both the present scheme and the argument outlined in [12] involve a significant extrapolation: the expressions for the pair potential and for the elastic free energy density are defined for all values of their independent variables, but become simple and easily comparable only for some special sets of configurations, usually in the limit of small angular displacements between vectors on neighbouring points. However, once the mapping has been obtained, the resulting equations for the pair potential are to be used in the general case of arbitrary mutual angular displacements.

Another mapping scheme can be found in a paper by Bedford and Windle [6]; their equations (17) to (20) for the pair potential are given by rational functions in the components of the unit vectors involved. As far as we could check, in the general case of different elastic constants, these equations are not written in terms of scalar products, and so are not gauge invariant. This was verified by considering the central unit vector to be aligned along the lattice z-axis, and the surrounding unit vector '6' (in the notation of [6]) to be its vertical neighbour, with components (ξ, η, ζ); then the pair interaction energy should reduce to a function of ζ only. However, after carrying out the appropriate substitutions, we found an irreducible dependence on ξ and η; our formulae manipulations were also checked by means of the computer algebra package Maple.

3. Simulation aspects

As for the choice of the parameters to be used for the two potential models, in [16] we have considered the comparatively simple and extensively studied nematogen 4,4′-dimethoxyazoxybenzene (*para*-azoxyanisole, PAA) and taken the values of its elastic constants at 120°C, which corresponds to a reduced temperature, T/T_{NI}, of 0.963, as reported in the book by de Gennes and Prost [2], i.e.

$$\begin{cases} K_1 = 7 \times 10^{-12}\,\mathrm{N} \\ K_2 = 4.3 \times 10^{-12}\,\mathrm{N} \\ K_3 = 17 \times 10^{-12}\,\mathrm{N}. \end{cases} \tag{38}$$

The coefficients λ, μ, ν, ρ, calculated from them were rescaled by dividing by $|\nu|$; the resulting pair potential, equation (13), hereafter referred to as Model 1 (M1), is

$$\Phi = \varepsilon\left\{\lambda[P_2(a_j) + P_2(a_k)] + \mu\left(a_j a_k b_{jk} - \frac{1}{9}\right) + \nu P_2(b_{jk}) + \rho[P_2(a_j) + P_2(a_k)]P_2(b_{jk})\right\} \tag{39}$$

with

$$\lambda = 0.79039, \quad \mu = -1.0611, \quad \nu = -1, \quad \rho = -0.43668. \tag{40}$$

Here ε (including the length Λ) is a positive quantity setting energy and temperature scales, i.e. $T^* = k_B T/\varepsilon$, and the scaled potential energy per particle is $U^* = U/(N\varepsilon)$. We now proceed in the same way for equation (37), and the resulting pair potential, hereafter referred to as Model 2 (M2), is the simpler function

$$\Phi = \varepsilon\left\{\lambda[P_2(a_j) + P_2(a_k)] + \mu\left(a_j a_k b_{jk} - \frac{1}{9}\right) + \nu P_2(b_{jk})\right\} \tag{41}$$

with

$$\lambda = 0.62791, \quad \mu = -5.3721, \quad \nu = -1. \tag{42}$$

As with M1, our study of M2 was aimed at elucidating the thermodynamic and structural behaviour of the bulk system. The simulations were carried out on cubic samples, using periodic boundary conditions with different sample sizes $N = q^3$, $q = 12, 16, 20, 24$, and closely correspond to those described in [16]. Each cycle (sweep) comprised $2N$ steps, and included sub-lattice sweeps. Note that, for each lattice site j, we can define the site parity $\chi_j = \pm 1$ depending on the sum of its coordinates being even or odd. That is, the lattice is bipartite, in that it consists of two interpenetrating sub-lattices of even and odd parities, where each site has six nearest-neighbour sites of the opposite parity, then twelve next-nearest neighbours of the same parity, and so on. Since the potential is restricted to nearest neighbours, there is no interaction between particles associated with lattice sites of the same parity, and so the outcomes of attempted Monte Carlo moves taking place at different sites of the same parity are independent of one another. We used a cycle consisting of N steps, where the tagged site was chosen randomly, followed by $N/2$ steps involving

lattice sites of one parity, and finally $N/2$ steps involving lattice sites of the other parity; this approach is found to be particularly efficient and has already been used both for magnetic [26, 27] and nematogenic lattice models [28, 29]. Calculations were carried out in cascade, in order of increasing temperature; equilibration runs took between 25 000 and 50 000 cycles, and production runs took between 100 000 and 250 000 cycles.

The quantities calculated from the simulation include the scaled potential energy per particle U^* and the configurational heat capacity which was determined as a fluctuation quantity; we also evaluated long range orientational order parameters of various ranks, $\bar{P}_L$, $L = 2, 4, 6$, and 8. The second and fourth rank orientational correlation coefficients and the singlet orientational distribution function were calculated at selected temperatures. The long range orientational order parameters are defined by [30, 31]

$$\bar{P}_L = \langle P_L(\cos\theta)\rangle, \quad L = 2, 4, 6, 8 \tag{43}$$

where θ is the angle between an individual molecule and the director; they were obtained in the following way. Along the Monte Carlo chain we calculated both the second rank tensor

$$Q_{\alpha\beta} = (3\langle u_\alpha u_\beta\rangle_{\text{loc}} - \delta_{\alpha\beta})/2 \tag{44}$$

and its fourth rank counterpart [30–33]; here the subscript loc refers to the current configuration, and the Greek subscripts label cartesian components. These quantities were accumulated to give macrostep averages, then used to calculate $\bar{P}_{2,\text{macr}}$ and $\bar{P}_{4,\text{macr}}$, as discussed elsewhere [30–34]. In addition, for every sweep the current second rank ordering tensor was diagonalized, and the instantaneous director $\mathbf{v}$ identified with the eigenvector associated with the eigenvalue possessing the largest magnitude; we then calculated the quantities $\langle P_L(\mathbf{u}\ \mathbf{v})\rangle_{\text{loc}}$ and averaged them. Since the director is known for the current configuration, this can also be used to calculate the singlet orientational distribution function [30, 31, 34, 35]. A 1001 bin histogram of $f(\theta)$ versus $|\cos\theta|$ was calculated at $T^* = 2.35$ and for a system size of $q = 20$. The underlying symmetry of the nematic phase means that this quantity is an even function of $\cos\theta$, and that the angle can be restricted between 0 and $\pi/2$; it can, therefore, be expanded as

$$f(\theta) = \frac{1}{2}\left[1 + \sum_{L\geqslant 0,\text{even}} (2L+1)\bar{P}_L P_L(\cos\theta)\right]. \tag{45}$$

The orientational correlation coefficients [30, 31] are defined by

$$G_L(r) = \langle P_L(\mathbf{u}_j\ \ \mathbf{u}_k)\rangle, \quad L = 2, 4 \tag{46}$$

and are functions of the (dimensionless) interparticle separation $r = |\mathbf{p}_j - \mathbf{p}_k|$. These computationally expensive quantities were calculated at two temperatures, i.e. $T^* = 2.35$ and 2.45 and again for $q = 20$, by analysing one configuration every fourth sweep; as we shall see, their plots show a rapid decay to a limiting value consistent with the corresponding order parameter, i.e.

$$\lim_{r\to\infty} G_L(r) = \bar{P}_L^2. \tag{47}$$

The short range order parameters [31]

$$\sigma_L = G_L(r=1) = \langle P_L(\mathbf{u}_j\ \ \mathbf{u}_k)\rangle \tag{48}$$

determined at the nearest-neighbour separation, were evaluated at all temperatures, by analysing one configuration every cycle; σ_2 is not related to the potential energy in any simple way, in contrast with the Lebwohl–Lasher model, where there is a direct proportionality between the two quantities.

4. Results and comparisons

Before presenting our simulation results, it is helpful to recall some molecular field predictions, to be used for comparison with them [36–39]. Upon summing over the six allowed orientations of the intermolecular vector both λ and ρ terms vanish, and the resulting potential of mean torque is given for both potential models by

$$\tilde{W} = 2W_0^*\bar{P}_2 P_2(\cos\theta), \quad W_0^* = [3\nu + (2/3)\mu], \tag{49}$$

where θ denotes the angle between an individual molecule and the director, and $\bar{P}_2$ is the second rank order parameter. The corresponding nematic–isotropic transition temperature given by the molecular field theory is $2|W_0^*|0.2202/k_B$.

We note that, for both potential models, W_0^* is the energy per particle of the configuration (Γ) where all particles are parallel to a lattice vector $\mathbf{e}_\alpha$. Let us also point out that, for a given pair potential model, this molecular field approach may or may not be qualitatively correct (see an example in [23]), depending on the numerical values of the coefficients; in other words, the configuration Γ may but need not be the ground state; however it is the ground state for the potential models M1 and M2. For M1, the ground state energy U_0^* found for the values for μ and ν (see equation (40)) is -3.7074, and so the corresponding transition temperature predicted by molecular field theory is $T_{\text{NI,MF}}^* = 1.6327$, compared with 1.3212 for the Lebwohl–Lasher model (the change in notation from W_0^* to U_0^* reflects the scaling by ε). The other molecular field predictions for the transitional properties are $\Delta S_{\text{MF}}^{\text{NI}}/R = 0.417$, $\bar{P}_{2,\text{MF}}^{\text{NI}} = 0.429$, $\bar{P}_{4,\text{MF}}^{\text{NI}} = 0.120$, for the transitional entropy, second and fourth rank order parameters, respectively [36–39]. In the case of M2, the values of μ and ν yield $U_0^* = -6.5814$, and thus $T_{\text{NI,MF}}^* = 2.8984$.

The simulation results for the potential energy and the configurational heat capacity are plotted in figures 1

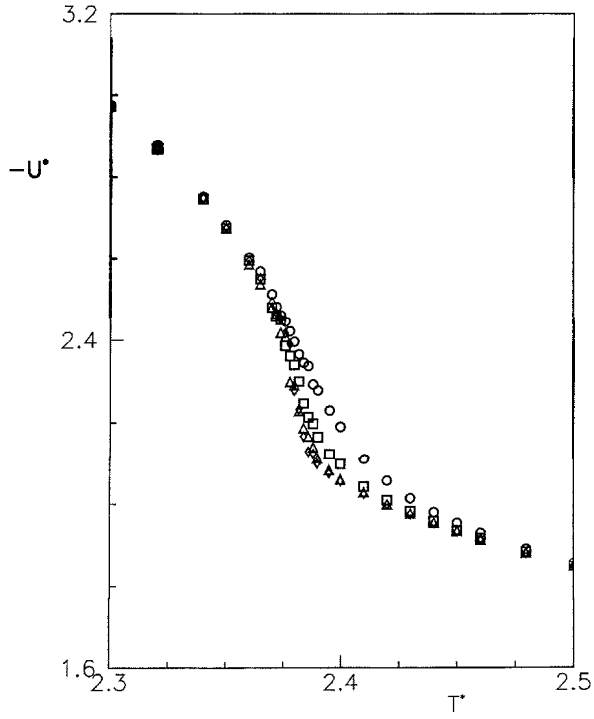

Figure 1. M2: simulation results for the potential energy, obtained with different sample sizes. Circles: $q = 12$; squares: $q = 16$; triangles: $q = 20$; diamonds: $q = 24$; the associated statistical errors fall within symbol sizes.

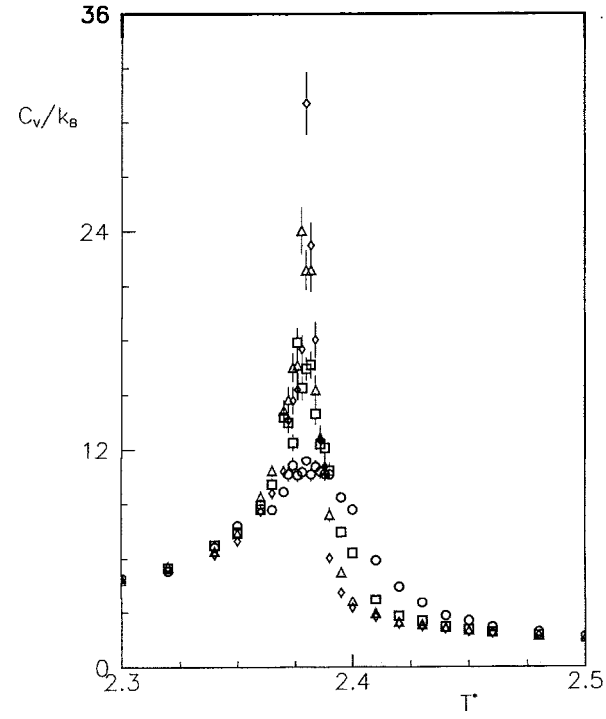

Figure 2. M2: simulation results for the configurational heat capacity, obtained with different sample sizes. Circles: $q = 12$; squares: $q = 16$; triangles: $q = 20$; diamonds: $q = 24$.

and 2; they are found to be independent of sample size for $T^* \leqslant 2.36$, then show a pronounced dependence on the system sizes up to $T^* \approx 2.42$, and again become independent of the sample size above this temperature. A small temperature step of 0.002 was used in the range between $T^* = 2.37$ and 2.39: here the heat capacity exhibits a maximum, growing narrower and higher as the sample size increases, and this is consistent with a first order transition [31]; the energy results over the same range are also consistent with a weak discontinuity at the transition.

The results for the order parameters, obtained by analysing one configuration every cycle, are plotted in figures 3 and 4; they are roughly independent of sample size up to $T^* \approx T_1^* = 2.378$, and show a pronounced decrease with sample size above this temperature. Their counterparts obtained via macrostep ordering tensors $\bar{P}_{2,\mathrm{macr}}$ and $\bar{P}_{4,\mathrm{macr}}$ (not reported here) exhibit the same qualitative trend; in the region $T^* \leqslant T_1^*$, there is a good agreement between the two sets of results; in contrast, above this temperature, $\bar{P}_{2,\mathrm{macr}}$ and $\bar{P}_{4,\mathrm{macr}}$ decrease more rapidly with increasing temperature and sample size; this comparison helps to locate the transition temperature. The results for $\bar{P}_6$ and $\bar{P}_8$ (not reported here) are much smaller (for example, at $T^* = 2.3$, $\bar{P}_6$ is about 0.02,

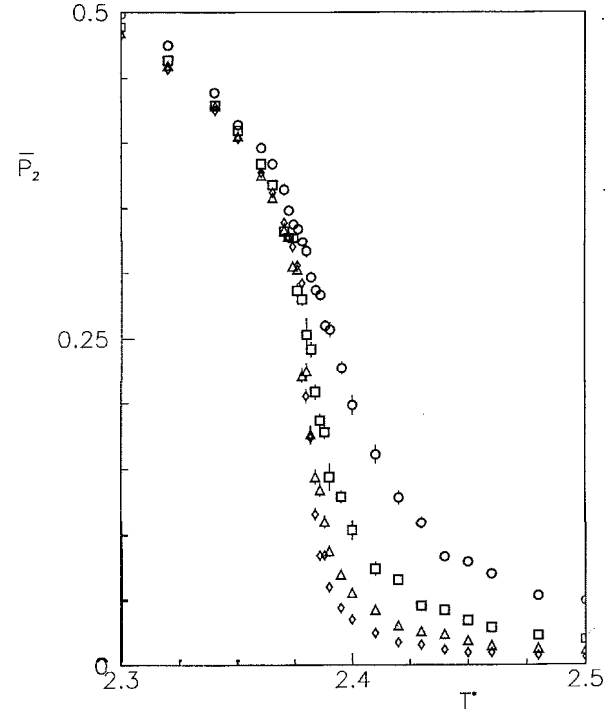

Figure 3. M2: simulation results for the second rank order parameter, obtained with different sample sizes. Circles: $q = 12$; squares: $q = 16$; triangles: $q = 20$; diamonds: $q = 24$.

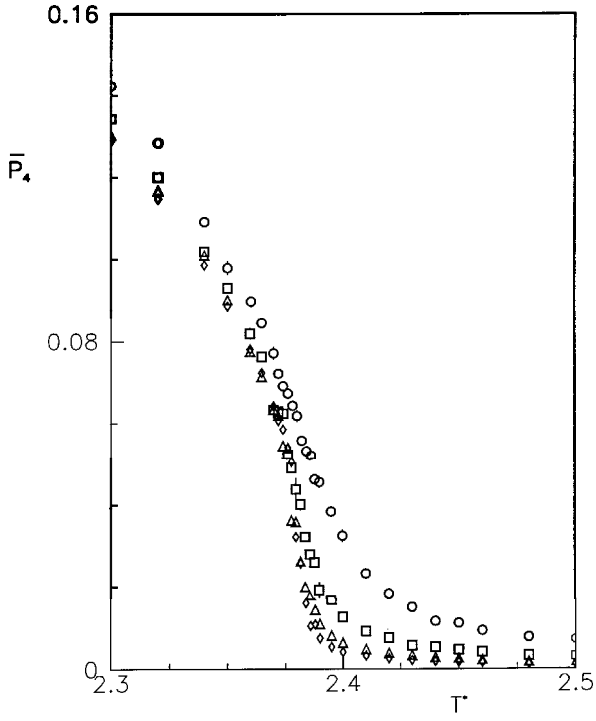

Figure 4. M2: simulation results for the fourth rank order parameter, obtained with different sample sizes. Circles: $q = 12$; squares: $q = 16$; triangles: $q = 20$; diamonds: $q = 24$.

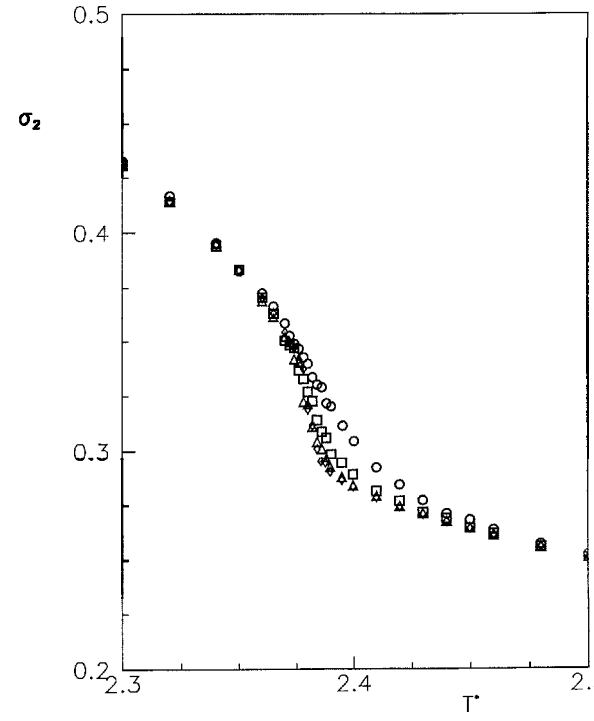

Figure 5. M2: simulation results for the short range order parameter σ_2 [see equation (48)], obtained with different sample sizes. Circles: $q = 12$; squares: $q = 16$; triangles: $q = 20$; diamonds: $q = 24$.

and $\bar{P}_8$ is about 0.002), and seem to go continuously to zero with increasing temperature.

Results for the short range order parameters σ_2 and σ_4 are plotted in figures 5 and 6, respectively; their sample-size dependences follow the pattern displayed by the potential energy. We also mention that, both for M1 [16] and M2, the plots of σ_4 versus σ_2 (not reported here) are linear to a good approximation.

These results are consistent with a comparatively weak first order transition between a nematic and an isotropic phase. To discuss this it is helpful to define the three temperatures $T_1^* = 2.378$, $T_2^* = 2.380$, $T_3^* = 2.382$, and the associated potential energies U_1^*, U_2^*, U_3^* for $q = 24$. The system is in the ordered phase for $T^* \leqslant T_1^*$, and in the disordered phase for $T^* \geqslant T_3^*$; we propose the intermediate temperature T_2^*, i.e. the abscissa of the peak of the heat capacity, as the transition temperature. The uncertainty in this is conservatively taken to be the temperature step used in the simulation, i.e. $T_{NI}^* = 2.380 \pm 0.002$. We also take $0.5(U_3^* - U_1^*)$ as a crude estimate of the energy jump at the phase transition. As a rough estimate for the order parameters at the nematic–isotropic transition $\bar{P}_2^{NI}$ and $\bar{P}_4^{NI}$, we propose the average of their values for $q = 24$ at the temperatures T_1^* and T_2^*. Our estimates for the transitional properties

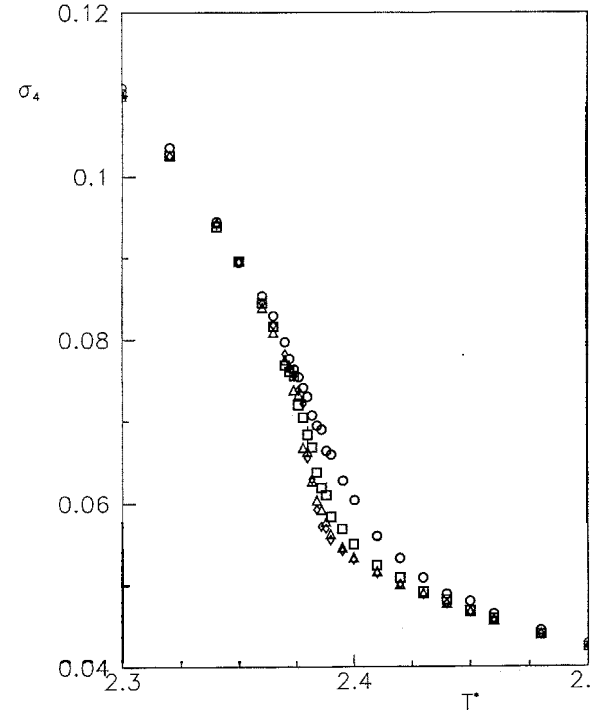

Figure 6. M2: simulation results for the short range order parameter σ_4, obtained with different sample sizes. Circles: $q = 12$; squares: $q = 16$; triangles: $q = 20$; diamonds: $q = 24$.

obtained in this way are then

$$T^*_{NI} = 2.380 \pm 0.002$$
$$\Delta U^*_{NI} = 0.079 \pm 0.006$$
$$\Delta S^{NI}/R = 0.033 \pm 0.003$$
$$\bar{P}_2^{NI} = 0.25 \pm 0.01$$
$$\bar{P}_4^{NI} = 0.041 \pm 0.002.$$

The corresponding quantities for the analogous M1 model are [16]

$$T^*_{NI} = 1.368 \pm 0.002$$
$$\Delta U^*_{NI} = 0.066 \pm 0.005$$
$$\Delta S^{NI}/R = 0.048 \pm 0.004$$
$$\bar{P}_2^{NI} = 0.26 \pm 0.01$$
$$\bar{P}_4^{NI} = 0.045 \pm 0.002.$$

For comparison, we also give here simulation estimates for the transitional properties of the Lebwohl–Lasher model, obtained by other authors and for q ranging up to 50 (a preliminary report of simulations carried out with $q = 120$ has been published [40]); $T^*_{NI} = 1.1232 \pm 0.0001$ [28, 32, 41–43]; $\Delta U^*_{NI} = 0.20 \pm 0.04$ and hence $\Delta S^{NI}/R = 0.18 \pm 0.04$ [42]; notice that [32] proposes $\Delta S^{NI}/R \leqslant 0.05$, which is in better accord with our results for models M1 and M2. Estimates reported for $\bar{P}_2^{NI}$ are 0.27 [32], 0.39 [42], and 0.17 [43], whereas $\bar{P}_4^{NI}$ has been estimated to be 0.04 [32]. These numbers show that, even in such an extensively studied model, an accurate characterization of the transition is still a difficult task [42].

The ratio between simulation and molecular field estimates for the transition temperature of the present model is 0.821, versus the corresponding value of 0.850 for the Lebwohl–Lasher model, and 0.837 for M1 [16]. We also note that the ground state energies of M1 and M2 are rather different, and that the ratio between simulation estimates for the transition temperatures nearly equals the ratio for the ground state energies, as expected from the molecular field theory. The two models M1 and M2 differ from each other and from the simpler Lebwohl–Lasher model by sizeable terms, only some of which contribute to the potential of mean torque; yet, as a net result, these additional terms in the potential make comparatively little difference to the transition temperature, moving it only slightly away from the molecular field limit.

The singlet orientational distribution function calculated at $T^* = 2.35$, for $q = 20$, is plotted in figure 7, and shows the expected maximum when $\cos\theta$ is unity.

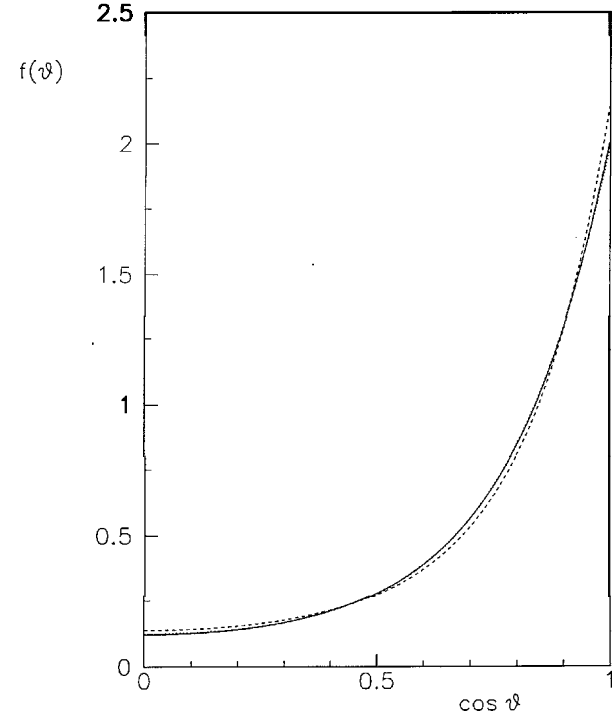

Figure 7. M2: results for the singlet orientational distribution function $f(\theta)$ at $T^* = 2.35$. Continuous curve: simulation results; dashed line: $f_{ME,2}$, see equation (50); dotted line: $f_{ME,4}$, see equation (51), hardly distinguishable from the continuous one. The relative statistical errors on the simulation results range up to 0.2%.

To check the quantitative aspects of this, the first four order parameters were calculated by convoluting the appropriate Legendre polynomials with this distribution function, and found to be

$$\bar{P}_2 = 0.406 \pm 0.002$$
$$\bar{P}_4 = 0.095 \pm 0.001$$
$$\bar{P}_6 = 0.013 \pm 0.001$$
$$\bar{P}_8 = 0.0013 \pm 0.0001.$$

The corresponding values $\bar{P}_{2,loc}$ and $\bar{P}_{4,loc}$ obtained by analysing a configuration every cycle, as explained in the previous section, agreed with the ones listed here to three significant figures. These results for $\bar{P}_2$ to $\bar{P}_8$ were used to construct a truncated expansion of the singlet orientational distribution function, including terms up to $\bar{P}_8$, and this turned out to be indistinguishable from the simulation results, to the resolution of the figure. An alternative route to $f(\theta)$ is via the maximum entropy approach [44–46]; if only the second rank order parameter is known, then the distribution function takes the form

$$f_{ME,2}(\theta) \propto \exp[c_2' P_2(\cos\theta)], \qquad (50)$$

whereas, if both $\bar{P}_2$ and $\bar{P}_4$ are available, then

$$f_{ME,4}(\theta) \propto \exp[c_2'' P_2(\cos\theta) + c_4'' P_4(\cos\theta)]. \quad (51)$$

Let us recall that order parameters of higher rank are not normally available experimentally; $\bar{P}_2$ is the dominant one, and the next term $\bar{P}_4$ is significantly smaller.

The proportionality factors in equations (50) and (51) allow for the normalization conditions of the distribution function, and the c parameters were determined by appropriate consistency constraints, i.e. by requiring $f_{ME,2}$ to reproduce $\bar{P}_2$, or requiring $f_{ME,4}$ to reproduce both $\bar{P}_2$ and $\bar{P}_4$ [44–46]. The results of this fitting process are shown in figure 7; the overall goodness of the resulting fit to the simulation results was defined quantitatively by calculating both the sum of squares of deviations (ξ) and the sum of squares of relative deviations (η). Their values for the M1 distribution function at $T^* = 1.35$ were found to be [16]

$$c_2' = 1.838, \quad \xi_2 = 0.527, \quad \eta_2 = 3.065 \quad (52)$$

and

$$c_2'' = 1.903, \quad c_4'' = -0.116; \quad \zeta \equiv c_4''/c_2'' = -0.061,$$
$$\xi_4 = 0.071, \quad \eta_4 = 0.053. \quad (53)$$

For the M2 model which we have studied

$$c_2' = 1.829, \quad \xi_2 = 0.807, \quad \eta_2 = 4.453 \quad (54)$$

and

$$c_2'' = 1.903, \quad c_4'' = -0.136; \quad \zeta = -0.071,$$
$$\xi_4 = 0.015, \quad \eta_4 = 0.072. \quad (55)$$

Together with these numerical results, figure 7 shows that $f_{ME,2}(\theta)$ yields a good but not quite perfect agreement with simulation results, and that $f_{ME,4}(\theta)$ produces a recognizable improvement. A qualitatively similar situation has been observed for the Lebwohl–Lasher model, where c_4'' is also negative, and about 8% of c_2'' [16, 32].

The orientational correlation coefficients $G_2(r)$ and $G_4(r)$, calculated at two typical temperatures $T^* = 2.35$ (nematic) and $T^* = 2.45$ (isotropic), are plotted in figure 8, as a function of the separation r; the logarithmic scale was chosen in order to compact four curves while still being able to distinguish between them. All of the four cases exhibit a rather steep decay of correlations between $r = 1$ and $r = \sqrt{3}$, then a recognizable increase at $r = 2$, and eventually monotonic decay at larger distances. This behaviour has been observed with other short range lattice models [16, 29, 32], whereas a monotonic decay at all distances has been obtained for lattice models with long range interactions [47].

Comparison between the properties of the models M1, M2 and the Lebwohl–Lasher model (see the Appendix

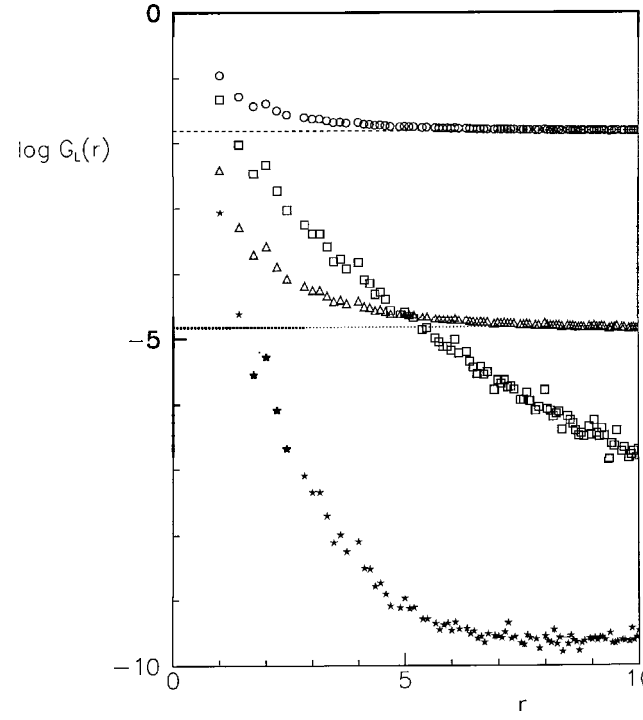

Figure 8. M2: simulation results for the logarithms of the orientational correlation coefficients at two different temperatures. Circles: $\log G_2(r)$ at $T^* = 2.35$ (nematic); squares: $\log G_2(r)$ at $T^* = 2.45$ (isotropic), triangles: $\log G_4(r)$ at $T^* = 2.35$ (nematic); stars: $\log G_4(r)$ at $T^* = 2.45$ (isotropic). The dashed line corresponds to $\log \bar{P}_2^2$ at $T^* = 2.35$, and the dotted one to $\log \bar{P}_4^2$ at the same temperature.

in [32]) can be carried out by plotting their appropriate simulation results versus the reduced temperature T^*/T^*_{NI}. The results for the potential energy are also scaled by the corresponding molecular field ground state energies U_0^*. We note that, both for M1 and M2, only the simulation results obtained with the largest system $q = 24$ have been used in this comparison, and that the simulation results for the Lebwohl–Lasher model from [32] were obtained with $q = 30$. The results for the potential energy are compared in figure 9, and show recognizable quantitative differences, which are correlated with the estimated value of the jump in the potential energy at the transition ΔU^*_{NI}. In contrast, comparisons for the configurational heat capacity—figure 10, the long range orientational order parameters—figure 11, and the short range order parameters σ_{2L}—figure 12, show a rather close agreement between M1 and M2, and a slightly larger difference between them and the Lebwohl–Lasher model. This is perhaps to be expected, because, although all of the models contain the dominant term in $P_2(b_{jk})$, models M1 and M2, unlike the Lebwohl–Lasher model, have in addition, terms involving the orientation of molecules with respect to the intermolecular vector.

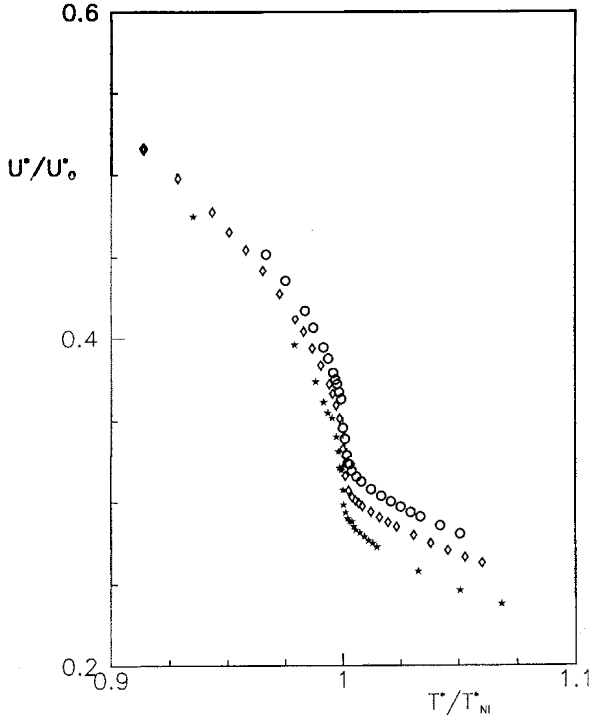

Figure 9. Simulation results for U^*/U_0^* versus T^*/T_{NI}^*, based on the different potential models. Diamonds: M1 [16]; circles: M2; stars: results for the Lebwohl–Lasher lattice model [32].

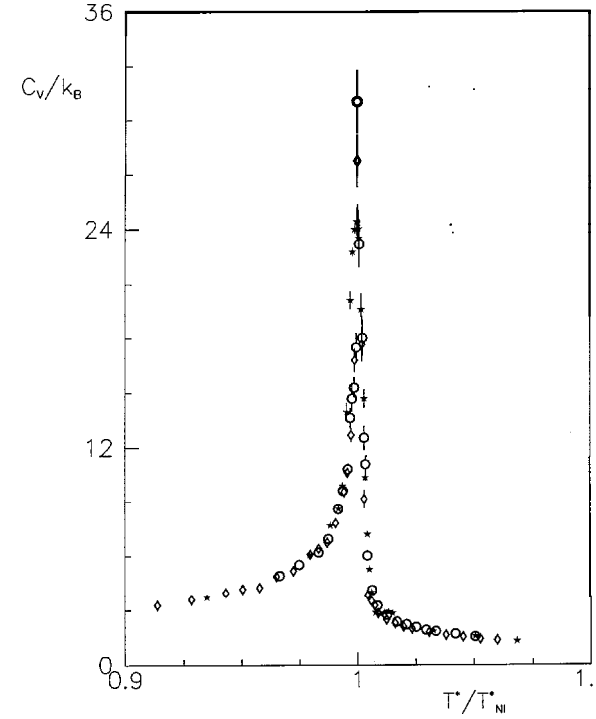

Figure 10. Simulation results for the configurational heat capacity versus the reduced temperature T^*/T_{NI}^*, obtained for the different potential models. Diamonds: M1 [16]; circles: M2; stars: results for the Lebwohl–Lasher lattice model [32].

Another, less severe, comparison of predictions for the structural properties can also be obtained by plotting $\bar{P}_4$ versus $\bar{P}_2$ [32], thus eliminating the explicit temperature dependences of the order parameters, as we have done in figure 13. The molecular field prediction can be continued to values $\bar{P}_2 < \bar{P}_{2,MF}^{NI}$ by means of the maximum entropy approximant $f_{ME,2}$, i.e. by using equation (50) to calculate both $\bar{P}_2$ and $\bar{P}_4$ for a range of values of c_2' [32]. The results show a fair qualitative agreement between the predictions and the results obtained for the three models, especially in the ordered region. The failure to obtain complete agreement presumably results from the importance of the fourth rank term in the potential of mean torque, see equation (51).

Since the nematogen 4,4′-dimethoxyazoxybenzene was involved in the choice of the elastic constants, we have also attempted comparison with its experimental properties. However, we emphasize that, because of the underlying simplifications in the models (i.e. the assumption of rigid and cylindrically symmetric molecules, and the neglect of translational degrees of freedom), only a qualitative agreement is to be expected [48]; similar comparisons for the Lebwohl–Lasher model can be found in [43, 48]. Among the properties of interest to us are the nematic–isotropic transition temperature, which is in the range 407–409 K [49–51], the enthalpy of transition, which ranges between 0.5 and 0.8 kJ mol^{-1} [3, 51–53]; taking a value for ΔH_P of 0.57 kJ mol^{-1}, the entropy change at constant pressure $\Delta S_P/R$ is estimated to be 0.19 ± 0.01 [3, 47, 51, 52], and from it the transition entropy at constant volume $\Delta S_V/R$ is found to be about 0.05. In addition, the order parameters $\bar{P}_2^{NI}$ and $\bar{P}_4^{NI}$ at the transition have been determined to be 0.39 and 0.08, respectively [54]. In terms of comparisons between model prediction and experimental results, these quantities are of two kinds, i.e. some of them depend on the scaling parameter ε in the model potential, that is T_{NI} and ΔH_P, whereas others do not, namely $\bar{P}_2^{NI}$, $\bar{P}_4^{NI}$ and $\Delta S_V/R$. We begin with those which do not require a knowledge of ε. Thus the models, both M1 and M2 as well as that of Lebwohl and Lasher, are in good agreement with the small experimental transitional entropy at constant volume of 0.05. The order parameters obtained for the three models are significantly lower than the experimental values [54] of 0.39 for $\bar{P}_2^{NI}$ and 0.08 for $\bar{P}_4^{NI}$. This difference could indicate the likely fact that the model pair potentials do not reflect the true anisotropic interactions between two PAA molecules, but might also result from the difficulty of locating the phase transition precisely in the simulations, combined with the strong and apparently continuous dependence of the order

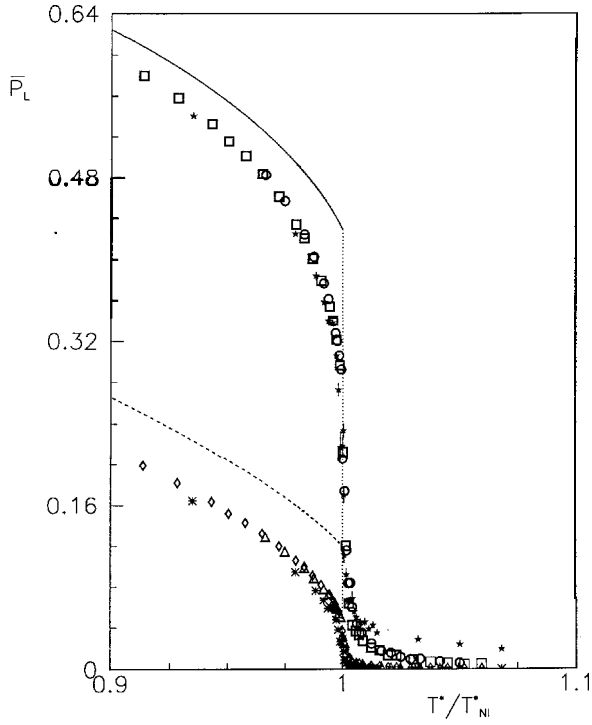

Figure 11. Simulation results for $\bar{P}_2$ and $\bar{P}_4$ versus the reduced temperature T^*/T^*_{NI}, obtained for the different potential models. Squares: $\bar{P}_2$ for M1; circles: $\bar{P}_2$ for M2; stars: $\bar{P}_2$ for the Lebwohl–Lasher lattice model [32]; diamonds: $\bar{P}_4$ for M1; triangles: $\bar{P}_4$ M2; asterisk: $\bar{P}_4$ for the Lebwohl–Lasher lattice model [32]. The predictions of the molecular field theory are shown as the solid line for $\bar{P}_2$ and the dashed line for $\bar{P}_4$.

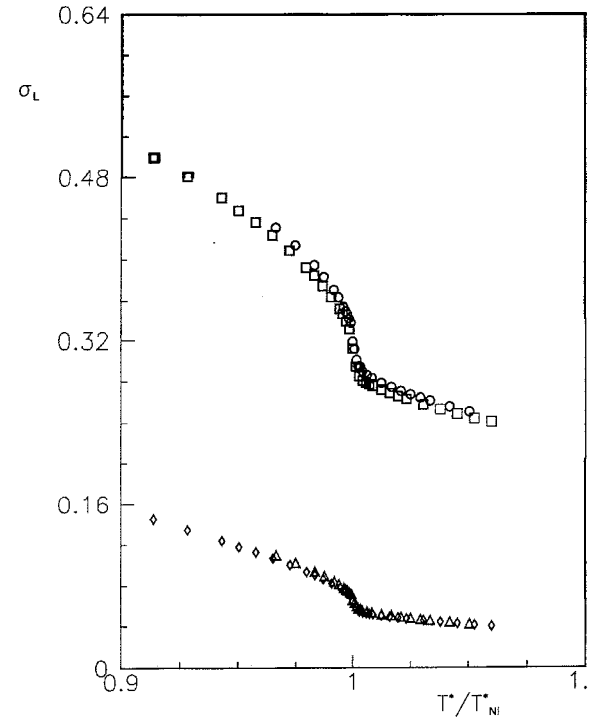

Figure 12. Simulation results for the short range order parameters σ_2 and σ_4 versus T^*/T^*_{NI}, obtained for the different potential models. Squares: σ_2 for M1; circles: σ_2 for M2; diamonds: σ_4 for M1; triangles: σ_4 M2.

parameters on temperature in the vicinity of the phase transition, see figures 3, 4 and 11.

To make a comparison with T_{NI} and ΔH_P we need to be able to estimate the scaling parameter ε. This can be achieved by choosing Λ, for which we take the cube root of the molar volume: values for the density of nematic 4,4′-dimethoxyazoxybenzene at room pressure reported in the literature range between 1.140 and 1.190 g cm^{-3} [49–51], so that the corresponding values for Λ have a narrow range between 7.1 and 7.2 Å. It is worth noticing that a change of temperature can cause a significant variation in the elastic constants, and hence in the prediction of the transition temperature; this could be used to improve the agreement with a particular model. The simulation estimate for M1 yields a transition temperature ranging between 546 and 538 K; the simulation estimate for ΔU_{NI} would then correspond to 0.22 kJ mol^{-1}. On the other hand, the estimated transition temperature for M2 ranges between 357 and 351 K, and ΔU_{NI} corresponds to 0.1 kJ mol^{-1}. Finally, if the three elastic constants are set to a common value (their average), then the transition temperature for the Lebwohl–Lasher lattice model [28, 32, 41–43], combined with experimental densities, yields estimates for the nematic–isotropic transition temperature ranging between 554 and 546 K; the simulation estimates in [42] give $\Delta U_{NI} = 0.82$ kJ mol^{-1}.

To conclude, our simulation results show a close qualitative similarity between models M1 and M2, a somewhat worse agreement with the simpler Lebwohl–Lasher model, and a broad qualitative agreement with experiment (see also more detailed comparisons in [16]); they also suggest that tailoring the pair potential to the specific nematogen yields a slightly better description of it, within these limitations.

The present extensive calculations were carried out, on, among other machines, a cluster of DEC computers belonging to the Sezione di Pavia of Istituto Nazionale di Fisica Nucleare (INFN); allocation of computer time by the Computer Centre of Pavia University and CILEA (Consorzio Interuniversitario Lombardo per l'Elaborazione Automatica, Segrate, Milan), as well as by CINECA (Centro Interuniversitario Nord-Est di Calcolo Automatico, Casalecchio di Reno, Bologna), within the INFM initiative on parallel computing, is also gratefully acknowledged. This collaborative project

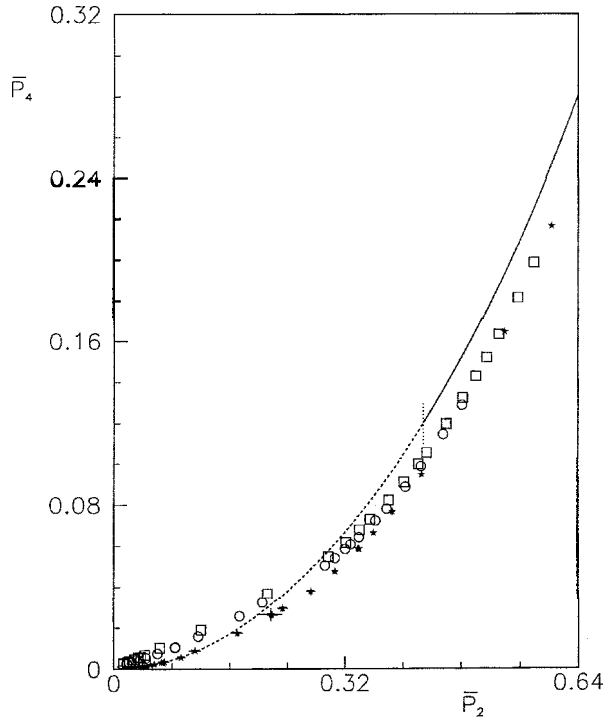

Figure 13. Plot of $\bar{P}_4$ versus $\bar{P}_2$, obtained for the different potential models. Squares: M1; circles: M2; stars: Lebwohl–Lasher lattice model [32]. Continuous line: molecular field prediction; dashed line: continuation of the molecular field curve to $\bar{P}_2 \leqslant \bar{P}_{2,\mathrm{MP}}^{\mathrm{NI}}$ (see also text); the dotted vertical line marks the separation between the two curves.

was discussed during visits of GRL to Pavia University, funded by grants allocated by the British Council and the Italian CNR, and then by INFM; S.R. also wishes to thank Prof. S. Hess for inviting him for a short visit to Berlin, supported by Deutsche Forschungsgemeinschaft under Sonderforschungsbereich SFB 335 'Anisotrope Fluide'. The present research was also partially funded by Minestero dell'Università e della Ricerca Scientifica e Tecnologica (MURST) through Cofin MURST 97 CFSIB.

Appendix

S-Functions

The pair potential for uniaxial molecules can be written quite generally as an expansion in a basis of S-functions [17–19], which conveniently separates the distance and orientation dependence of the potential. That is,

$$W(r, \Omega) = \sum_{J,K,L} w_{JKL}(r) S_{JKL}(\Omega), \tag{A1}$$

where r is the intermolecular separation and Ω denotes the orientations of the two molecules and the intermolecular vector. For molecules with a centre of symmetry, the summation involves only even values of J, K and L, with L in the range $|J-K|$ to $(J+K)$. The S-functions are defined by

$$S_{JKL}(\Omega) = (i)^{J-K-L} \sum_{n,p,M} \begin{pmatrix} J & K & L \\ n & p & M \end{pmatrix} C_{Jn}(\omega_j) C_{Kp}(\omega_k) \times C_{LM}(\omega_r) \tag{A2}$$

where $C_{Jn}(\omega_j)$ is a modified spherical harmonic, ω_j denotes the spherical coordinates of the symmetry axis of molecule j in a laboratory frame, and $\begin{pmatrix} J & K & L \\ n & p & M \end{pmatrix}$ is a $3j$ symbol. Although this form of the S-functions is particularly convenient when transforming between axis systems [18, 19], it is not so convenient when numerical values of the pair potential are needed, as in computer simulation. However, the S-functions can be expressed in terms of the cartesian components of the unit vectors $\mathbf{u}_j$, $\mathbf{u}_k$ and $\mathbf{r}$, for the molecular symmetry axes and the intermolecular vector, respectively. In this form the S-functions depend on the three scalar products a_j, a_k and b_{jk} defined in equation (12); the first few of them are

$$S_{000}(\Omega) = 1 \tag{A3a}$$

$$S_{202}(\Omega) = \frac{1}{2\sqrt{5}}(3a_j^2 - 1) \tag{A3b}$$

$$S_{022}(\Omega) = \frac{1}{2\sqrt{5}}(3a_k^2 - 1) \tag{A3c}$$

$$S_{220}(\Omega) = \frac{1}{2\sqrt{5}}(3b_{jk}^2 - 1) \tag{A3d}$$

$$S_{222}(\Omega) = \frac{1}{\sqrt{70}}[2 - 3(a_j^2 + a_k^2 + b_{jk}^2) + 9a_j a_k b_{jk}] \tag{A3e}$$

$$S_{224} = \frac{1}{4\sqrt{70}}[1 + 2b_{jk}^2 + 5(-a_j^2 - a_k^2 - 4a_j a_k b_{jk} + 7a_j^2 a_k^2)] \tag{A3f}$$

$$S_{422} = \frac{1}{4\sqrt{70}}[1 + 2a_k^2 + 5(-a_j^2 - b_{jk}^2 - 4a_j a_k b_{jk} + 7a_j^2 b_{jk}^2)] \tag{A3g}$$

$$S_{242} = \frac{1}{4\sqrt{70}}[1 + 2a_j^2 + 5(-a_k^2 - b_{jk}^2 - 4a_j a_k b_{jk} + 7a_k^2 b_{jk}^2)]. \tag{A3h}$$

The S-functions form an orthonormal and complete set, and have various symmetry properties with respect to permutation of the subscripts [19]. The expansion coefficients $w_{JKL}(r)$ can be treated as adjustable parameters with which to fit a particular and only partly

determined model potential, as we have done in this paper; alternatively, they can be taken from a specific and fully determined molecular interaction, such as the dispersion potential [21]. We have chosen here to include only S-functions of low order, in the interest of simplicity. Comparisons with the polynomials τ_h in equations (8) to (11) show that each set of functions can be expressed as a linear combination of the others; of course the transformation formulae become complicated as one goes to higher and higher orders. We note, for example, that τ_2 in equation (9) is a combination involving $S_{000}(\Omega)$, $S_{202}(\Omega)$, $S_{022}(\Omega)$, and $S_{220}(\Omega)$, and that τ_3 involves $S_{222}(\Omega)$ as well. The ρ term in model M1 involves $S_{422}(\Omega)$ and $S_{242}(\Omega)$ also [19], whereas the potential model M2 is a linear combination involving $S_{220}(\Omega)$, $S_{202}(\Omega)$, $S_{022}(\Omega)$, $S_{222}(\Omega)$ only, and $S_{224}(\Omega)$ is involved in equation (15).

References

[1] Kapanowski, A., 1997, *Phys. Rev. E*, **55,** 7090.
[2] De Gennes, P. G., and Prost, J., 1995, *The Physics of Liquid Crystals*, 2nd Edn (Oxford: Oxford University Press).
[3] Chandrasekhar, S., 1992, *Liquid Crystals*, 2nd Edn (Cambridge: Cambridge University Press).
[4] Chandrasekhar, S., and Ranganath, G. S., 1986, *Adv. Phys.*, **35,** 507.
[5] Bedford, S. E., Nicholson, T. M., and Windle, A. H., 1991, *Liq. Cryst.*, **10,** 63.
[6] Bedford, S. E., and Windle, A. H., 1993, *Liq. Cryst.*, **15,** 31.
[7] Hobdell, J. R., and Windle, A. H., 1997, *Liq. Cryst.*, **23,** 157.
[8] Hobdell, J. R., and Windle, A. H., 1996, *Mat. Res. Soc. Symp. Proc.*, **425,** 131.
[9] Kilian, A., and Hess, S., 1989, *Z. Naturforsch. A*, **44,** 693.
[10] Kilian, A., and Hess, S., 1990, *Liq. Cryst.*, **8,** 465.
[11] Kilian, A., 1993, *Liq. Cryst.*, **14,** 1189.
[12] Gruhn, T., and Hess, S., 1996, *Z. Naturforsch. A*, **51,** 1.
[13] Liu, C., and Muthukumar, M., 1997, *J. chem. Phys.*, **106,** 7822.
[14] Lebwohl, P. A., and Lasher, G., 1972, *Phys. Rev. A*, **5,** 1350.
[15] Lasher, G., 1972, *Phys. Rev. A*, **6,** 426.
[16] Romano, S., 1998, *Int. J. mod. Phys. B*, **12,** 2305.
[17] Blum, L., and Torruella, J. L., 1972, *J. chem. Phys.*, **56,** 303.
[18] Stone, A. J., 1979, *The Molecular Physics of Liquid Crystals*, edited by G. R. Luckhurst and G. W. Gray (London: Academic Press), Chap. 2, pp. 31–50.
[19] Stone, A. J., 1978, *Mol. Phys.*, **36,** 241.
[20] Humphries, R. L., Luckhurst, G. R., and Romano, S., 1981, *Mol. Phys.*, **42,** 1205.
[21] London, F., 1937, *Trans. Faraday Soc.*, **33,** 8.
[22] De Boer, J., 1942, *Physica*, **9,** 363.
[23] Romano, S., 1988, *Liq. Cryst.*, **3,** 323.
[24] Barbero, G., and Evangelista, L. R., 1997, *Phys. Rev. E*, **56,** 6189.
[25] Nehring, J., and Saupe, A., 1972, *J. chem. Phys.*, **56,** 5527.
[26] Ferrenberg, A., and Landau, D. P., 1991, *Phys. Rev. B*, **44,** 5081.
[27] Peczak, P., and Landau, D. P., 1993, *Phys. Rev. B*, **47,** 14 260.
[28] Greff, C. W., and Lee, M. A., 1994, *Phys. Rev. E*, **49,** 3225.
[29] Romano, S., 1995, *Int. J. mod. Phys. B*, **9,** 85.
[30] Zannoni, C., 1979, *The Molecular Physics of Liquid Crystals,* edited by G. R. Luckhurst and G. W. Gray (London: Academic Press), Chap. 3, pp. 51–84.
[31] Zannoni, C., 1979, *The Molecular Physics of Liquid Crystals*, edited by G. R. Luckhurst and G. W. Gray (London: Academic Press), Chap. 9, pp. 191–220.
[32] Fabbri, U., and Zannoni, C., 1986, *Mol. Phys.*, **58,** 763.
[33] Chiccoli, C., Pasini, P., Biscarini, F., and Zannoni, C., 1988, *Mol. Phys.*, **65,** 1505.
[34] Romano, S., 1987, *Europhys. Lett.*, **2,** 431; Romano, S., 1987, *Nuovo Cim. D*, **9,** 409.
[35] Romano, S., 1992, *Liq. Cryst.*, **12,** 641.
[36] Maier, W., and Saupe, A., 1958, *Z. Naturforsch. A*, **13,** 564; Maier, W., and Saupe, A., 1959, *Z. Naturforsch. A*, **14,** 882; Maier, W., and Saupe, A., 1960, *Z. Naturforsch. A*, **15,** 287.
[37] Luckhurst, G. R., 1979, *The Molecular Physics of Liquid Crystals*, edited by G. R. Luckhurst and G. W. Gray (London: Academic Press), Chap. 4, pp. 85–120.
[38] Zannoni, C., 1979, *Mol. Cryst. liq. Cryst. Lett.*, **49,** 247.
[39] Van der Haegen, R., Debruyne, R., Lyckx, R., and Lekkerkerker, H. N. W., 1980, *J. chem. Phys.*, **73,** 2469.
[40] Boschi, S., Brunelli, M. P., Zannoni, C., Chiccoli, C., and Pasini, P., 1997, *Int. J. mod. Phys. C*, **8,** 547.
[41] Zhang, Z., Mouritsen, O. G., and Zuckermann, M. J., 1992, *Phys. Rev. Lett.*, **69,** 2803.
[42] Zhang, Z., Zuckermann, M. J., and Mouritsen, O. G., 1993, *Mol. Phys.*, **80,** 1195.
[43] Gonin, D., and Windle, A. H., 1997, *Liq. Cryst.*, **23,** 489.
[44] Jaynes, E. T., 1957, *Phys. Rev.*, **106,** 620; Jaynes, E. T., 1957, *Phys. Rev.*, **108,** 171.
[45] Levine, R. D., and Tribus, M. (editors), *The Maximum Entropy Formalism* 1979, Cambridge, Mass: M.I.T. Press).
[46] Bower, D. I., 1981, *J. Polym. Sci. Polym. Phys.*, **19,** 93.
[47] Angelescu, N., Romano, S., and Zagrebnov, V. A., 1995, *Int. J. mod. Phys. B*, **9,** 859.
[48] Luckhurst, G. R., and Simpson, P., 1982, *Mol. Phys.*, **47,** 251.
[49] *Beilsteins Handbuch der Organischen Chemie*, 1974, drittes Ergänzungswerk, 16. Band (Berlin: Springer).
[50] Stephen, M. J., and Straley, J. P., 1974, *Rev. mod. Phys.*, **46,** 617.
[51] Martire, D. E., 1979, *The Molecular Physics of Liquid Crystals*, edited by G. R. Luckhurst and G. W. Gray (London: Academic Press), Chap. 10, pp. 221–238.
[52] Domalski, E. S., and Hearing, E. D., 1990, *J. phys. Chem. ref. Data*, **19,** 881.
[53] Acree, W. E., Tucker, S. A., Pilcher, G., Paz de Andrade, M., and Ribeiro da Silva, M. D. M. C., 1993, *J. chem. Thermodyn.*, **25,** 653.
[54] Hamley, I. W., Garnett, S., Luckhurst, G. R., Roskilly, S. J., Skov Pedersen, J., Richardson, R. M., and Seddon, J. M., 1996, *J. chem. Phys.*, **104,** 10 046.